Translational Oncology
www.transonc.com

Volume 9 Number 3 June 2016 pp. 219–227 219

Evaluating Changes to Blood-Brain Barrier Integrity in Brain Metastasis over Time and after Radiation Treatment[1]

Donna H. Murrell*,†, Niloufar Zarghami†, Michael D. Jensen†, Ann F. Chambers†,‡, Eugene Wong†,‡ and Paula J. Foster*,†

*Imaging Research Laboratories, Robarts Research Institute, London, ON, Canada; †Department of Medical Biophysics, Schulich School of Medicine and Dentistry, Western University, London, ON, Canada; ‡London Regional Cancer Program, London Health Sciences Centre, London, ON, Canada

Abstract

INTRODUCTION: The incidence of brain metastasis due to breast cancer is increasing, and prognosis is poor. Treatment is challenging because the blood-brain barrier (BBB) limits efficacy of systemic therapies. In this work, we develop a clinically relevant whole brain radiotherapy (WBRT) plan to investigate the impact of radiation on brain metastasis development and BBB permeability in a murine model. We hypothesize that radiotherapy will decrease tumor burden and increase tumor permeability, which could offer a mechanism to increase drug uptake in brain metastases. *METHODS:* Contrast-enhanced magnetic resonance imaging (MRI) and high-resolution anatomical MRI were used to evaluate BBB integrity associated with brain metastases due to breast cancer in the MDA-MB-231-BR-HER2 model during their natural development. Novel image-guided microirradiation technology was employed to develop WBRT treatment plans and to investigate if this altered brain metastatic growth or permeability. Histology and immunohistochemistry were performed on whole brain slices corresponding with MRI to validate and further investigate radiological findings. *RESULTS:* Herein, we show successful implementation of microirradiation technology that can deliver WBRT to small animals. We further report that WBRT following diagnosis of brain metastasis can mitigate, but not eliminate, tumor growth in the MDA-MB-231-BR-HER2 model. Moreover, radiotherapy did not impact BBB permeability associated with metastases. *CONCLUSIONS:* Clinically relevant WBRT is not curative when delivered after MRI-detectable tumors have developed in this model. A dose of 20 Gy in 2 fractions was not sufficient to increase tumor permeability such that it could be used as a method to increase systemic drug uptake in brain metastasis.

Translational Oncology (2016) 9, 219–227

Introduction

The relative 5-year survival for breast cancer patients has steadily increased and was recently reported at 90% in the United States [1]. Now, the major challenge of this disease is its ability to metastasize to distant sites where detection and therapy become complicated. The incidence of metastasis to the brain is especially high for women with breast cancer that overexpresses the human epidermal growth factor receptor 2 (HER2) and has been reported at 25% to 48% [2–4]. More concerning is that brain metastases often manifest while metastases outside of the brain are still responding to successful anti-HER2 therapies, such as trastuzumab (Herceptin). Several factors may be involved in this type of mixed response, including

Address all correspondence to Donna H. Murrell, Imaging Research Laboratories, Robarts Research Institute, 1151 Richmond St. North, London, ON, Canada, N6A 5B7. E-mail: dmurrell@robarts.ca

[1] Funding for this project was provided by Canadian Institutes of Health Research in the form of an Operating Grant awarded to P. J. F. (principal applicant) and A. F. C. and E. W. (coapplicants).

Received 18 February 2016; Revised 11 April 2016; Accepted 23 April 2016

1936-5233/16
http://dx.doi.org/10.1016/j.tranon.2016.04.006

the unique microenvironment of the brain, neuroinflammation, and genetic alterations distinct from the primary tumor [5,6]. Notably, the inability of traditional systemic therapies to penetrate the intact blood-brain barrier (BBB) to any significant degree, or at all, presents a significant obstacle for drug delivery, thus rendering the brain a sanctuary site for metastatic growth [7,8].

In the absence of effective systemic therapy, treatment options for patients with brain metastases are limited; they include steroids, surgical excision of solitary metastases, stereotactic radiosurgery for small lesions not amenable to surgery, and whole brain radiotherapy (WBRT). Although combinations of these options have improved prognosis, the median survival time of patients with HER2+ breast cancer is only 11.5 to 16.5 months after diagnosis of brain metastasis [9]. The clinical standard for treating multiple [e.g. more than three lesions detected by magnetic resonance imaging (MRI)] brain metastases and diffuse disease is WBRT; however, this treatment is palliative. Response to treatment may be improved by optimizing the timing of radiotherapy in combination with systemic therapies. Some studies suggest that radiation can increase vascular permeability within tumors and in healthy brain tissue [10,11]. If WBRT increases permeability of the local BBB *in vivo*, it may be possible to increase drug uptake in brain metastases and improve on the results of systemic therapy or radiotherapy alone [12].

Several contrast agents with varying sizes have been used to assess BBB integrity and degree of permeability. Under normal conditions, the intact BBB prevents extravasation of contrast agents. Damage to the BBB can therefore be evaluated based on the size, charge, and composition of contrast agents that are able to cross the BBB and accumulate in the brain. Traditionally, BBB permeability has been studied by microscopy using agents such as sodium fluorescin (376 Da), Texas red dextran (3 or 70 kDa), horseradish peroxidase (44 kDa), or albumin-bound Evans blue dye (69 kDa) [8,10,13–15]. These techniques are limited by their *ex vivo* nature, inability to monitor changes over time, and contrast agent sizes that are not directly relevant to drug uptake. In this work, we evaluate BBB integrity *in vivo* over time using gadolinium-enhanced (Gd) MRI, which is routinely used in clinical diagnosis to identify BBB breakdown.

Gd-enhanced MRI has also been used in preclinical cancer models to evaluate BBB permeability associated with brain tumors [14,16–19]. Regions where the BBB has been compromised can be visualized because of local accumulation of the Gd contrast agent, which results in signal enhancement (brightness) in the image. Using this method, substantial heterogeneity has been reported in the permeability of brain metastases. In addition, both Gd-permeable as well as Gd-impermeable tumors have been observed within the same brain [17,19]. Notably, Percy and colleagues also found that many metastases were impermeable to Gd early in development but became permeable over time [17]. Here, we build on these results by investigating whether radiation therapy increases the permeability of brain metastases to understand if it is possible to open a window where systemic therapy could have increased efficacy.

In this study, we developed a clinically relevant WBRT treatment protocol that is feasible in the MDA-MB-231-BR-HER2 experimental brain metastatic breast cancer model. We used this model along with contrast-enhanced MRI and high-resolution anatomical MRI to investigate the impact of clinically relevant radiation treatment on the growth of brain metastases due to breast cancer and on BBB integrity in a murine model. We hypothesized that radiotherapy will decrease the tumor burden in treated animals and increase tumor permeability.

Methods

Cell Culture

The brain metastatic breast cancer cells (MDA-MB-231-BR-HER2) used in this research were a kind gift from Dr. Patricia Steeg's laboratory at the National Cancer Institute (Bethesda, MA) [20,21]. Cells were grown in Dulbecco's modified Eagle's medium with 10% fetal bovine serum and 1% penicillin and streptomycin, and were maintained at 37°C and 5% CO_2. The cell line was tested for mycoplasma contamination using the MycoAlert Mycoplasma Detection Kit (Lonza, Rockland, ME) and was found to be negative. The trypan blue exclusion assay was used to determine cell viability.

Animal Preparation

Female nude mice (nu/nu, aged 6-8 weeks from Charles River Laboratories, Wilmington, MA) were housed in a pathogen-free barrier facility at Robarts Research Institute. All experiments were approved by the Animal Use Subcommittee of the University Council on Animal Care at the University of Western Ontario. Mice ($n = 2$ for commissioning, $n = 12$ for WBRT experiment) were anesthetized with 2% isoflurane in oxygen and given an intracardiac injection of 100,000 MDA-MB-231-BR-HER2 cells suspended in 0.1 ml of Hank's balanced salt solution. Mice were euthanized by an overdose injection of pentobarbital (Euthanyl) after the final imaging session.

Radiotherapy

We previously developed an integrated micro-computed tomography (CT)/RT system capable of sophisticated image-guided conformal small-animal radiotherapy [22]. The microirradiation technology is based on a modified preclinical micro-CT system (GE eXplore CT 120, GE Healthcare, Milwaukee, WI) with an upgraded x-ray generator (140 kVp, 50 kW), custom irradiation control software (Parallax-Innovations, London, ON, Canada), and a custom-built computer-controlled collimator. Thus far, it had been used for respiratory-gated rat lung irradiation and was commissioned for mouse WBRT in this work [22,23]. Mice were anesthetized (1.5% isoflurane in oxygen), placed feet first prone on the rodent couch, and aligned using setup lasers and CT imaging. On-board fluoroscopy was used to identify the skull and position computerized collimators such that the whole brain was targeted for irradiation and the remainder of the head and body was shielded. Animal temperature was maintained using a heating pad, and breathing rate was monitored during treatment.

Magnetic Resonance Imaging

Magnetic resonance images were acquired on a 3.0-T GE Excite MR750 clinical scanner (General Electric, Mississauga, ON, Canada) using a custom-built gradient insert coil (inner diameter = 17.5 cm, gradient strength = 500 mT/m, and peak slew rate = 3000 T/m per second). Mice were anesthetized (1.5% isoflurane in oxygen) and placed in a custom solenoidal mouse head radiofrequency coil (inner diameter = 1.5 cm). Animal temperature was maintained using warm saline bags during imaging. Anatomical balanced steady-state free precession (bSSFP) scans were acquired with the following parameters: spatial resolution = 100 × 100 × 200 μm, repetition time = 8 milliseconds, echo time = 4 milliseconds, flip angle = 35°, signal averages = 2, radiofrequency phase cycles = 8, and scan time =

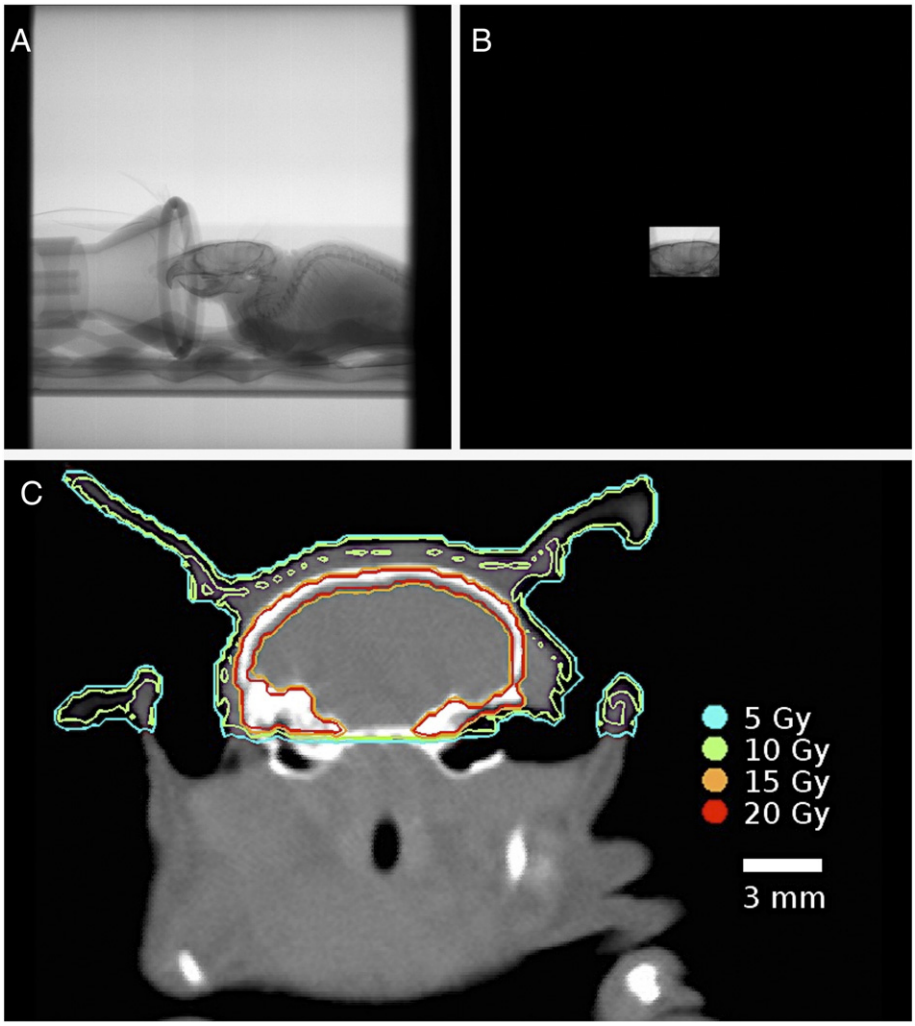

Figure 1. Micro-CT/RT targeting for mouse WBRT. Fluoroscopy-guided collimation of the mouse brain (A, B) allows for precise delivery of the 10-Gy per fraction treatment plan. Dosimetry was verified using a Monte Carlo dose calculation, where the 10-Gy isodose line is delineated in green (C). The brain received a uniform dose of 10 Gy. Enhanced dose to the skull is observed due to the low energy of the beam (140 kV) where photoelectric effect is prominent.

29 minutes. ZIP2 and ZIP512 upscaling was applied. Post-Gd T1-weighted spin echo (T1w SE) images were acquired at approximately 45 minutes after an intraperitoneal injection of 0.2 ml gadopentetate dimeglumine (Magnevist, 0.5 mmol/ml). The parameters were spatial resolution = 156 × 156 × 400 μm, repetition time = 600 milliseconds, echo time = 20 milliseconds, signal averages = 8, and scan time = 20 minutes. ZIP512 upscaling was applied.

Data Analysis

Open-source OsiriX image software (version 3.9.2) was used for image analysis. Brain metastases were counted, and the boundaries of each were manually segmented using the ROI tool in every bSSFP slice throughout the whole mouse brain. Tumor volume was then calculated by a three-dimensional reconstruction using the Osirix volume algorithm. Enhancing fraction (reflecting Gd-permeable tumors) was determined as previously described by comparing tumor detection in corresponding post-Gd T1w SE and bSSFP images [17,19]. Metastases that are detected in both the post-Gd T1w SE and the bSSFP sequences are considered "enhancing"; tumors appearing in only the bSSFP images are "nonenhancing." Tumors detected in bSSFP without a corresponding T1w SE image slice were excluded from the enhancement analysis.

Statistical analysis was performed using GraphPad Prism version 6.0 software (GraphPad, San Diego, CA). Where two groups were compared, two-way paired or unpaired Student's *t* tests were performed. Where two groups were compared over multiple time points, two-way repeated-measures analyses of variance were performed. For enhancement-related statistical analyses over time, one untreated mouse was removed because of unsuccessful injection on day 32; therefore, repeated measures were not used for this analysis. *Post hoc* analysis included Sidak's multiple-comparisons tests.

Histology and Immunohistochemistry

At experimental end point, mice were first perfused with 0.9% saline before perfusion fixation with 4% formalin. Brains were then excised and further fixed for 24 hours by immersion in 4% formalin. Fixed brains were then processed, paraffin embedded, and cut into 5 μm sections. Brain sections were then stained with hematoxylin and eosin (H&E) for morphology, or immunohistochemistry was performed for either the proliferation marker Ki67, or for human mitochondria markers (clone

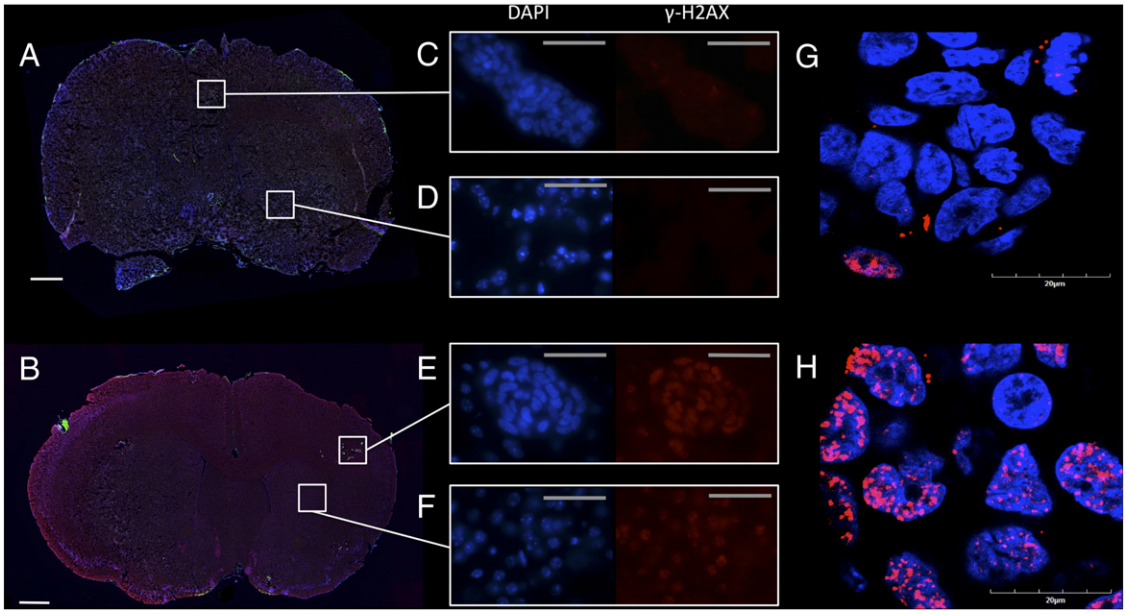

Figure 2. Response to radiation-induced DNA DSB was visualized by fluorescent γ-H2AX immunohistochemistry. This staining was performed 30 minutes postradiotherapy with fluorescent γ-H2AX (red foci) on a nuclear DAPI background (blue) on whole brain sections of untreated (A) and WBRT-treated (B) mouse brain. Magnified images of untreated tumor (C) and normal brain (D) showed minimal γ-H2AX signal intensity compared with irradiated tumor (E) and irradiated normal brain (F). Confocal microscopy illustrated that the accumulation of γ-H2AX was within the nuclei of tumor cells; untreated nuclei had few intrinsic γ-H2AX foci (G), and treated nuclei had many γ-H2AX foci in response to radiation-induced DNA DSB. Scale bars are 750 μm (A,B), 50 μm (C–F), and 20 μm (G,H).

MTCO2). Briefly, Ki67 staining was achieved on selected brain sections using heat-mediated antigen retrieval with citrate buffer pH 6. Tissue sections were blocked with Dako Protein Block, Serum-Free (Dako Canada, Inc., Burlington, ON, Canada), and incubated with anti-ki67 (1:100, ab833, Abcam Inc.) rabbit polyclonal antibodies. Positive staining was detected using Dako LSAB2 system-HRP (Dako Canada Inc.) and Vector DAB peroxidase substrate kit (Vector Laboratories, Burlingame, CA) according to manufacturer's instructions. Mouse anti-human mitochondria antibody (clone MTCO2, 1:100) was used with the Dako Animal Research Kit according to manufacturer's instructions for detection of human cells. All sections were counterstained with hematoxylin.

For commissioning studies, mice were perfused with 0.9% saline before perfusion fixation with 4% paraformaldehyde; brains were excised, further fixed for 24 hours by immersion in 4% formalin, placed in ascending sucrose gradients (10%, 20%, 30%), embedded in optimal cutting temperature compound (Tissue-Tek, Sakura, Torrance, CA), frozen, cryosectioned with 10-μm thickness, and stained by immunohistochemistry for γ-H2AX using the Ford protocol [24]. Sections were incubated with mouse anti–γ-H2AX antibody (1:700, anti–phospho-histone H2AX, Ser139, clone JBW301; Millipore, Billerica, MA) overnight and then stained with secondary antibody Alexa-Fluoro 594 goat anti-mouse IgG (1:500, Life Technologies, Carlsbad, CA) for 1 hour at room temperature. All sections were counterstained with 4',6-diamidino-2-phenylindole (DAPI) and mounted with antifade medium Vectashield (Vector Laboratories, Inc., Burlington, ON, Canada).

All staining was imaged on an Axio Imager A1 microscope (Zeiss CANADA, Toronto, ON, Canada) with a Retiga EXi (QImaging Scientific Research Cameras, Surrey, BC, Canada) digital camera. Whole brain histology images were acquired using the TISSUEscope 4000 (Huron Digital Pathology, Waterloo, ON, Canada). For γ-H2AX confocal images, an inverted confocal microscope (Olympus Fluoview FV1000 Confocal Imaging System) was used.

Results

Radiation Therapy Planning and Verification

First, the integrated micro-CT/RT system used in this research was implemented for mouse WBRT. A treatment plan of 20 Gy in two fractions on consecutive days was decided based on the biological effective dose to tumor (assuming $\alpha/\beta = 10$) to be equivalent to the clinical WBRT dose fractionation scheme of 30 Gy/10. Image guidance allowed for precise isolation of the mouse brain in a collimated 10 × 14–mm field; fluoroscopy images show the uncollimated field (Figure 1*A*) and collimated field (Figure 1*B*). The brain was irradiated with two identical fields using a parallel-opposed beam setup. One beam was delivered from the animal's left-right direction and one from right-left, for a cumulative dose of 10 Gy per fraction. A Monte Carlo dose verification calculation was performed to confirm delivery of the treatment plan (10 Gy is shown by a green line) (Figure 1*C*). Mean dose rate was 0.12 ± 0.01 Gy/min.

Immunohistochemistry was performed after irradiation to confirm adequate whole brain coverage by the radiotherapy plan. Irradiation-induced DNA damage response was verified by fluorescent γ-H2AX immunohistochemistry and the DAPI nuclear stain; this confirmed the actual whole brain radiation field in tissue. Whole brain sections bearing MDA-MB-231-BR-HER2 metastases were imaged with a fluorescent microscope at 10× magnification; these showed no damage to unirradiated mouse brain (Figure 2*A*) and

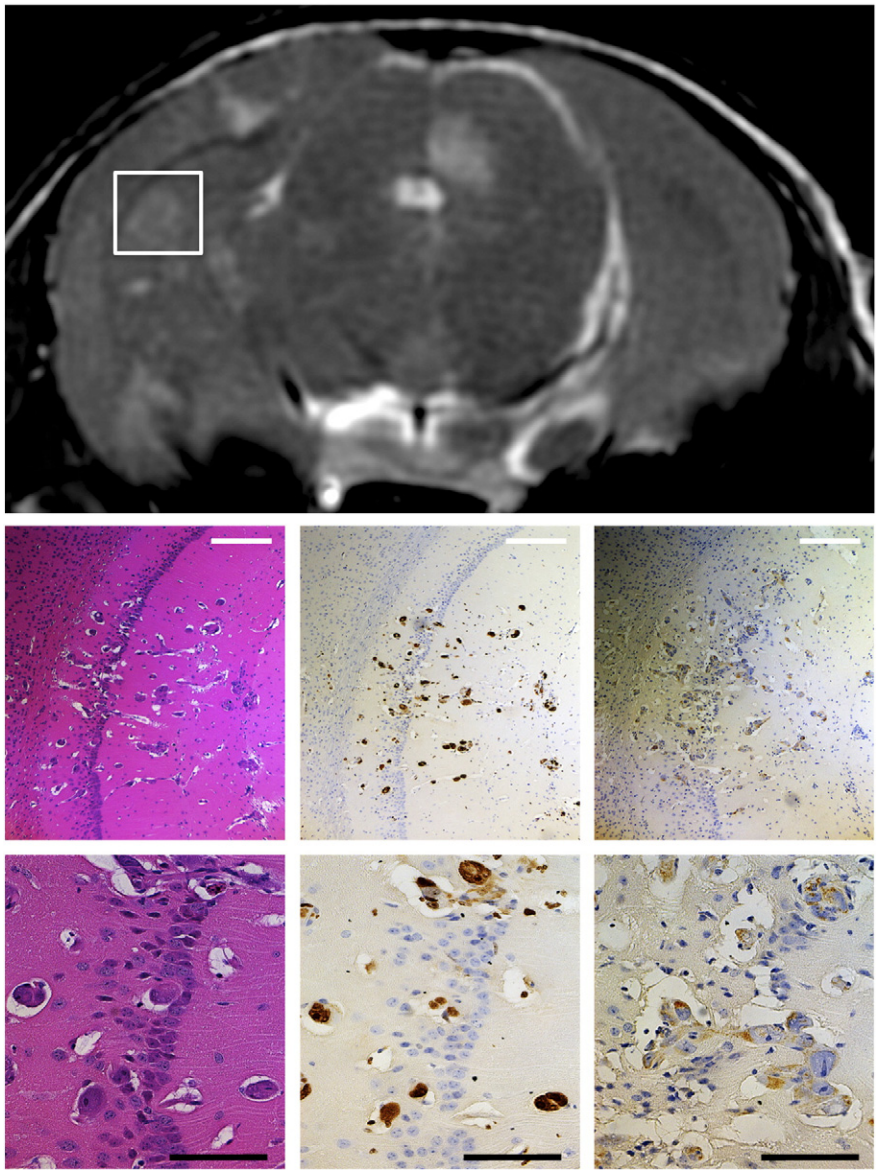

Figure 3. Representative MRI with correlative histology and immunohistochemistry of metastases in the MDA-MB-231-BR-HER2 brain metastasis model. Staining for H&E (left column), Ki67 (middle column), and human mitochondria (right column) at 10 × magnification (top row, white scale bar = 250 μm) and 40 × magnification (bottom row, black scale bar = 100 μm) supports the imaging data and confirmed that MRI-detected lesions were proliferative cancerous tumors of human origin.

confirmed homogeneous γ-H2AX response to radiation-induced DNA double-stranded breaks (DSB, red foci) across the whole treated mouse brain 30 minutes after the second fraction of 20 Gy/2 (Figure 2*B*). Intrinsic DNA DSB response was evaluated in 100× magnification images of tumor tissue and normal brain of an unirradiated mouse (Figure 2, *C* and *D*) and compared with initial DNA DSB response in a mouse brain 30 minutes postirradiation (Figure 2, *E* and *F*). Increased γ-H2AX intensity is evident in both tumor and normal brain tissue in the mouse brain treated with whole brain radiotherapy compared with untreated. Confocal microscopy confirms accumulation of γ-H2AX within the nuclei of tumor cells. Whereas few intrinsic γ-H2AX foci are present in nuclei of unirradiated tumor cells (Figure 2*G*), they are highly prevalent in response to DNA DSB at 30 minutes postirradiation (Figure 2*H*).

Brain sections were also assessed at end point (day 36 post–cell injection) to confirm imaging results, evaluate proliferation in tumors, and verify human status of the developing cancer (Figure 3). Hyperintense regions in the MRI corresponded to tumor regions as assessed by morphology in standard H&E histology. Ki67 staining of neighboring sections indicated that the detected tumors were proliferative. Staining for human mitochondria also confirmed that the metastases were of human origin. The histology and immunohistochemistry therefore validate that the MRI findings in this study reflect cancerous growth due to the injected MDA-MB-231-BR-HER2 cell line.

WBRT Experiment

Next, the micro-CT/RT system was used to deliver WBRT (20 Gy/2) to nude mice with brain metastatic breast cancer. Treatment

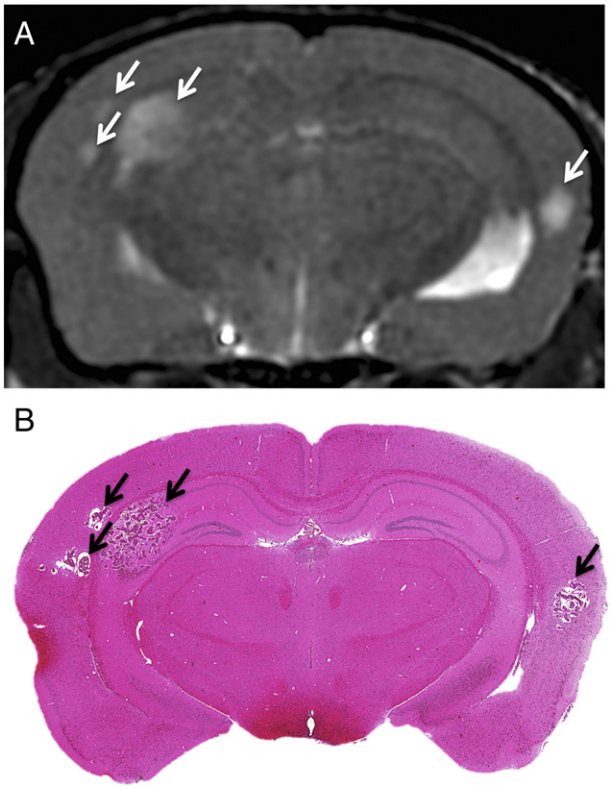

Figure 4. Representative images of metastases due to MDA-MB-231-BR-HER2 human brain metastatic breast cancer on day 36. bSSFP MRI illustrated metastasis burden by the appearance of hyperintensities (A), and this corresponded with tumor detection in H&E-stained sections (B).

was delivered when mice developed small MRI-detectable brain tumors (day 24 and 25 post–cell injection); this timing mimics the usual treatment following diagnosis that occurs in the clinic. Three dimensional, high-resolution anatomical bSSFP MRI was used to detect and monitor tumor progression over time. Radiological findings correspond well with tumor burden in whole brain histology sections (Figure 4).

The number of tumors, total tumor volume, and mean tumor volume over time (day 23, 32, and 36) were quantified in bSSFP images, and these data are presented in Table 1. WBRT did not have an effect on the number of tumors or on total tumor volume over time; however, it did have an effect on the mean volume of a tumor over time ($P < .01$); *post hoc* analysis found that mean tumor volume was significantly less in WBRT-treated mice than untreated ($P < .001$).

Substantial variability was observed in tumor response after WBRT. The changes in volume of 209 treated tumors were analyzed between 7 and 11 days posttreatment (day 32 and 36). A paired two-tailed *t* test found no significant difference between the fraction of tumors that decreased in volume after WBRT compared with the fraction that increased (Figure 5*A*). Furthermore, despite the same treatment plan, some mice had more tumors that decreased in volume after radiotherapy than others. For example, as shown in Figure 5*B*, 85% of the brain tumors in mouse B had a decreased volume after WBRT, whereas only 15% of the tumors in mouse E had a decreased volume after WBRT.

Next, BBB integrity was evaluated by determining the ability of Gd to accumulate within tumors and cause increased signal intensity (enhancement). Analysis of BBB permeability by enhancement in T1w SE post-Gd images was performed as previously described, and representative MR image slices of the same mouse brain are shown in Figure 6, *A* and *B* [17,19]. The enhancing fraction over time is shown in Figure 6*C*. Over time, a higher proportion of enhancing metastases are detectable in both groups ($P < .0001$). Of the nonenhancing tumors present in untreated mice (black bars) on day 32, 29% (9 of 31) changed to enhancing by day 36. Similarly, 26% (6 of 23) of nonenhancing tumors in WBRT mice (white bars) changed to enhancing in the same time frame. WBRT did not increase the fraction of enhancing tumors.

Temporal analysis of enhancement status and mean tumor volume (Figure 7) found that enhancing tumors grow larger than nonenhancing tumors over time in both untreated and WBRT-treated groups ($P < .001$ and $P < .01$, respectively). *Post hoc* analysis found that enhancing tumors are significantly larger than nonenhancing on day 32 and 36 in both groups (untreated: $^{\bullet\bullet}P < .05$, $^{\bullet}P < .0001$. WBRT: $^{\circ\circ}P < .0001$, $^{\circ}P < .0001$). Radiotherapy affected the growth of enhancing and nonenhancing tumors differently (Figure 7, *striped* versus *solid bars*). Over time, WBRT had an increased effect on the size of enhancing tumors ($P < .01$); *post hoc* analysis between treatment groups showed that the mean volume of enhancing tumors is significantly less in WBRT-treated mice compared with untreated on day 36 ($^{*}P < .0001$). Contrarily, time and treatment group did not affect the volume of nonenhancing tumors.

Discussion

This research used high-resolution anatomical and contrast-enhanced MRI in a murine model of breast cancer brain metastasis to monitor tumor development and permeability *in vivo*. This was combined with novel image-guided microirradiation technology to provide insight into the responses of tumors and alternations in BBB integrity in a clinically relevant model of breast cancer brain metastasis and WBRT.

Table 1. Quantification Tumor Incidence, Burden, and Mean Tumor Volume from MRI in the Traditional WBRT Experiment

Analysis	Day 23		Day 32		Day 36		Main Effect
	Untreated	WBRT	Untreated	WBRT	Untreated	WBRT	
Number of tumors	7.0 ± 11	25 ± 29	17 ± 19	34 ± 33	18 ± 19	34 ± 33	Time $P < .0001$
Total tumor volume (mm^3)	0.26 ± 0.41	0.98 ± 1.4	4.9 ± 5.8	8.3 ± 9.8	9.8 ± 11	8.4 ± 9.3	Time $P < .01$
Mean tumor volume (mm^3)	0.030 ± 0.022	0.035 ± 0.014	0.33 ± 0.18	0.23 ± 0.067	0.67 ± 0.40*	0.23 ± 0.059*	Interaction between time and treatment $P < .01$

The number of tumors and total tumor volume in the mouse brain increased over time from day 23 to 36, but there was no difference between treatment groups for these measurements. Traditional WBRT had a significant effect on mean tumor volume over time; *post hoc* analysis between groups indicated that, by day 36, on average, tumors were smaller in treated mice compared with untreated (*). Data are presented as mean ± SD. $N = 6$ for each group.

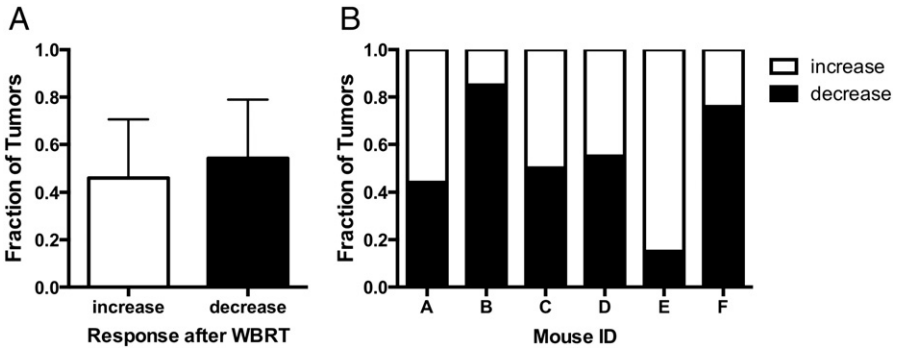

Figure 5. Treatment response was heterogeneous after traditional WBRT. There was no significant difference between the fraction of tumors that decreased in volume after traditional WBRT and the fraction that continued to increase (A). In addition, the response to therapy was markedly different for each mouse, ranging from 15% to 85% of the tumors in a mouse brain being reduced in tumor volume following treatment (B). Error bars are standard deviation.

A micro-CT/RT system with asymmetrical computerized jaws was successfully applied to deliver mouse whole brain irradiation. These are the first experiments where such a system has been used to demonstrate the effects of WBRT on brain metastatic development. This technology has the capacity to target and deliver conformal irradiation to the mouse brain via onboard image-guided collimation. Postirradiation, γ-H2AX staining confirmed that response to radiation-induced DNA DSB was present and was uniform across the whole mouse brain. Dose rate was low compared with other preclinical irradiators; however, doses up to 20 Gy per fraction can be delivered in one session, and increased dose can compensate for the lower dose rate [25,26]. Here, we chose 20 Gy/2 to keep side effects at a minimum while delivering biological effective doses that are relevant for WBRT.

Using this small-animal irradiation system, traditional WBRT was given after MRI detected tumors; this sequence, where treatment follows diagnosis, is the usual order of events in the clinic. WBRT was able to mitigate tumor growth, although it could not eliminate the

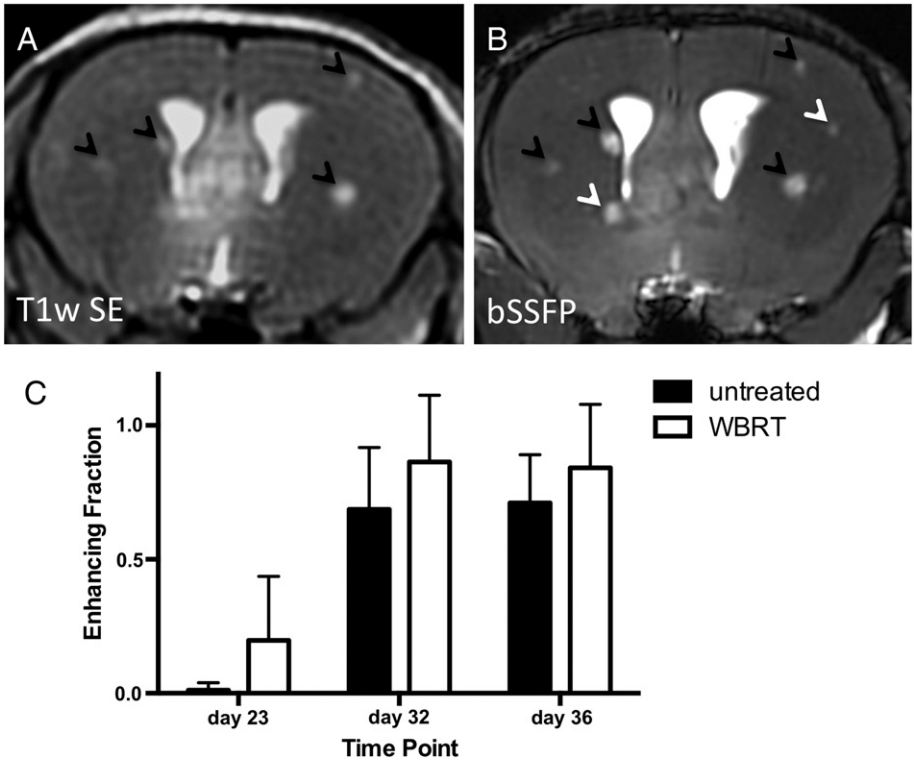

Figure 6. Tumor permeability visualized and quantified over time by contrast-enhanced MRI. Enhancing fraction (representing Gd-permeable tumors) was quantified as the number of enhancing tumors relative to total tumor burden by assessment of T1w SE post-Gd (A) and bSSFP images (B). Black arrows indicate metastases that were detected in both the T1w SE and the bSSFP sequences; these were considered "enhancing." White arrows indicate metastases that were detected in the bSSFP image but were absent in the corresponding post-Gd T1w SE image; these were considered "nonenhancing." Over time, the enhancing fraction increased in both groups; treatment did not have any significant effect (C). Error bars represent standard deviation.

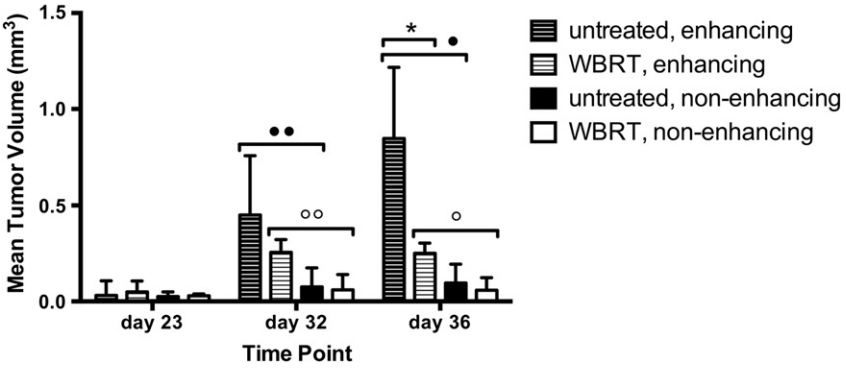

Figure 7. Enhancing and nonenhancing tumors respond differently to WBRT. In both untreated and WBRT-treated mice, enhancing tumors were larger than nonenhancing tumors at day 32 and at day 36 (statistical significance indicated by ••, •, °°, and °). By day 36, the mean volume of an enhancing tumor in a treated mouse was significantly less than untreated (*); however, there was no difference between groups in the volume of nonenhancing tumors. Error bars represent standard deviation.

tumor burden. Similar results were reported by Smart and colleagues who observed that fractionated (3 Gy × 10 fractions, starting on day 14 postinjection) or single-dose (15 Gy × 1 fraction on day 14) radiotherapy could reduce, but not eliminate, the number of large and micrometastases in the 231-BR experimental brain metastasis model [27]. In our study, the largest contributor to the drop in mean tumor volume of treated animals was a decrease in the mean volume of enhancing tumors. On the contrary, nonenhancing tumor volumes, although significantly less by comparison, were not different between treatment groups. Increased BBB permeability with tumor size, in addition to innate BBB heterogeneity, has been reported by several groups and investigated for its impact on systemic drug delivery [8,17,18,28,29]. However, to the best of our knowledge, this is the first report indicating that impermeable tumors may not respond to radiotherapy in the same way as their permeable counterparts.

Increased vascular permeability and BBB disruption after irradiation have been well documented [10,11,30]. This stimulated the idea that radiotherapy may be a useful mechanism to improve chemotherapeutic efficacy by increasing drug uptake though breakdown of the BBB, which is usually prohibitively exclusive to anticancer drugs. Yet, clinical studies investigating combinations of chemo- and radiotherapy remain inconclusive [31–33]. Previous studies may have offered poor insight due to limitations by their *in vitro or ex vivo* nature, nontranslational animal models, and irradiation doses that are not clinically relevant [10,11]. Moreover, no study has looked at these effects in the context of brain metastasis. Our study addresses all of these limitations; we used MRI tumor enhancement post-Gd administration to assess tumor permeability *in vivo* and found that the fraction of enhancing tumors was not different between treated and untreated mice at any time point. Furthermore, the percent of tumors that change from nonenhancing to enhancing was similar after WBRT compared with untreated. Notably, tumor enhancement post-Gd administration reflects sufficient BBB permeability to allow the 590-Da Gd-based contrast agent to cross; this is approximately the same molecular weight as lapatinib (581 Da), a dual tyrosine kinase inhibitor used in combination therapy for HER2+ metastatic breast cancer patients. Taskar and colleagues previously reported that limited BBB permeability in the vast majority of brain metastases contributed to poor therapeutic efficacy for this drug [28]. Our study, using Gd as a permeability marker, did not find a suitable mechanism to increase tumor permeability. Our results suggest that increased BBB permeability due to clinically relevant radiotherapy, as measured by enhancement post-Gd administration, is not present at 1 week or 11 days post-WBRT as was previously hypothesized [12]. Moreover, the idea that radiotherapy can increase BBB permeability and thereby improve drug delivery is not feasible in this model.

In summary, this research developed technology for image-guided mouse WBRT and used it with high-resolution anatomical and contrast-enhanced MRI to investigate tumor and BBB response after radiotherapy in a mouse model of breast cancer brain metastasis. Contrary to previous hypotheses, increased tumor permeability after radiotherapy was not found, although enhancing tumors decreased in volume after radiotherapy and nonenhancing tumors did not.

Competing Interests

The authors declare that they have no competing interests.

Authors' Contributions

D. H. M. carried out the MRI experiments, image analyses, statistical analyses, data interpretation, and histology and drafted the manuscript. D. H. M. also participated in study design, cell culture, and animal irradiation. N. Z. carried out the γ-H2AX immunohistochemistry and participated in animal irradiation. M. D. J. carried out the dose verification calculation and participated in animal irradiation. A. F. C., E. W., and P. J. F. conceived the study, participated in its design and coordination, and helped to draft the manuscript. All authors read and approved the final manuscript.

Acknowledgements

The authors thank Yuhua Chen, Carmen Simedra, Carl Postenka, Suzy Wong, and Amanda Hamilton for their assistance with immunohistochemistry, cell culture, and intracardiac injections.

D. H. M. is supported by a Fellowship funded by the Canadian Breast Cancer Foundation–Ontario Region, a Translational Breast Cancer Traineeship sponsored in part by the Breast Cancer Society of Canada, and the Canadian Institutes of Health Research Strategic Training Program in Cancer Research and Technology Transfer award. N. Z. is supported by a Translational Breast Cancer Traineeship sponsored in part by the Breast Cancer Society of

Canada. A. F. C. is a Canada Research Chair in Oncology supported by the Canada Research Chairs Program.

Funding for this project was provided by Canadian Institutes of Health Research in the form of an Operating Grant awarded to P. J. F. (principal applicant) and A. F. C. and E. W. (coapplicants).

The funders had no role in study design, acquisition and analysis of data, decision to publish, or preparation of the manuscript.

References

[1] Siegel R, Ma J, Zou Z, and Jemal A (2014). Cancer statistics, 2014. *CA Cancer J Clin* **64**, 9–29.

[2] Clayton AJ, Danson S, Jolly S, Ryder WDJ, Burt PA, Stewart AL, Wilkinson PM, Welch RS, Magee B, and Wilson G, et al (2004). Incidence of cerebral metastases in patients treated with trastuzumab for metastatic breast cancer. *Br J Cancer* **91**, 639–643.

[3] Bendell JC, Domchek SM, Burstein HJ, Harris L, Younger J, Kuter I, Bunnell C, Rue M, Gelman R, and Winer E (2003). Central nervous system metastases in women who receive trastuzumab-based therapy for metastatic breast carcinoma. *Cancer* **97**, 2972–2977.

[4] Lai R, Dang CT, Malkin MG, and Abrey LE (2004). The risk of central nervous system metastases after trastuzumab therapy in patients with breast carcinoma. *Cancer* **101**, 810–816.

[5] Lin NU, Amiri-Kordestani L, Palmieri D, Liewehr DJ, and Steeg PS (2013). CNS metastases in breast cancer: old challenge, new frontiers. *Clin Cancer Res* **19**, 6404–6418.

[6] Brastianos PK, Carter SL, Santagata S, Cahill DP, Jones RT, and Van Allen EM (2015). Genomic characterization of brain metastases reveals branched evolution and potential therapeutic targets. *Cancer Discov* **5**, 1164–1177.

[7] Stemmler H-J, Schmitt M, Willems A, Bernhard H, Harbeck N, and Heinemann V (2007). Ratio of trastuzumab levels in serum and cerebrospinal fluid is altered in HER2-positive breast cancer patients with brain metastases and impairment of blood-brain barrier. *Anticancer Drugs* **18**, 23–28.

[8] Lockman PR, Mittapalli RK, Taskar KS, Rudraraju V, Gril B, Bohn KA, Adkins CE, Roberts A, Thorsheim HR, and Gaasch JA, et al (2010). Heterogeneous blood-tumor barrier permeability determines drug efficacy in experimental brain metastases of breast cancer. *Clin Cancer Res* **16**, 5664–5678.

[9] Hayashi N, Niikura N, Masuda N, Takashima S, Nakamura R, Watanabe K, Kanbayashi C, Ishida M, Hozumi Y, and Tsuneizumi M (2015). Prognostic factors of HER2-positive breast cancer patients who develop brain metastasis: a multicenter retrospective analysis. *Breast Cancer Res Treat* **149**, 277–284.

[10] Li Y, Chen P, Haimovitz-friedman A, Reilly RM, and Wong CS (2003). Endothelial apoptosis initiates acute blood-brain barrier disruption after ionizing radiation; 2003 5950–5956.

[11] Fauquette W, Amourette C, Dehouck M-P, and Diserbo M (2012). Radiation-induced blood-brain barrier damages: an in vitro study. *Brain Res* **1433**, 114–126.

[12] van Vulpen M, Kal HB, Taphoorn MJB, and El-Sharouni SY (2002). Changes in blood-brain barrier permeability induced by radiotherapy: implications for timing of chemotherapy? *Oncol Rep* **9**, 683–688.

[13] Zhang R, Price JE, Fujimaki T, Bucana CD, and Fidler IJ (1992). Differential permeability of the blood-brain barrier in experimental brain metastases produced by human neoplasms implanted into nude mice. *Am J Pathol* **141**, 1115–1124.

[14] Connell JJ, Chatain G, Cornelissen B, Vallis K A, Hamilton A, Seymour L, Anthony DC, and Sibson NR (2013). Selective permeabilization of the blood-brain barrier at sites of metastasis. *J Natl Cancer Inst* **105**, 1634–1643.

[15] Yen LF, Wei VC, Kuo EY, and Lai TW (2013). Distinct patterns of cerebral extravasation by Evans blue and sodium fluorescein in rats. *PLoS One* **8**, 1–9.

[16] Song H-T, Jordan EK, Lewis BK, Liu W, Ganjei J, Klaunberg B, Despres D, Palmieri D, and Frank JA (2009). Rat model of metastatic breast cancer monitored by MRI at 3 tesla and bioluminescence imaging with histological correlation. *J Transl Med* **7**, 88.

[17] Percy DB, Ribot EJ, Chen Y, McFadden C, Simedrea C, Steeg PS, Chambers AF, and Foster PJ (2011). In vivo characterization of changing blood-tumor barrier permeability in a mouse model of breast cancer metastasis: a complementary magnetic resonance imaging approach. *Invest Radiol* **46**, 718–725.

[18] Thorsen F, Fite B, Mahakian LM, Seo JW, Qin S, Harrison V, Johnson S, Ingham E, Caskey C, and Sundstrøm T, et al (2013). Multimodal imaging enables early detection and characterization of changes in tumor permeability of brain metastases. *J Control Release* **172**, 812–822.

[19] Murrell DH, Hamilton AM, Mallett CL, van Gorkum R, Chambers AF, and Foster PJ (2015). Understanding heterogeneity and permeability of brain metastases in murine models of HER2-positive breast cancer through magnetic resonance imaging: implications for detection and therapy. *Transl Oncol* **8**, 176–184.

[20] Yoneda T, Williams PJ, Hiraga T, Niewolna M, and Nishimura R (2001). A bone-seeking clone exhibits different biological properties from the MDA-MB-231 parental human breast cancer cells and a brain-seeking clone in vivo and in vitro. *J Bone Miner Res* **16**, 1486–1495.

[21] Palmieri D, Bronder JL, Herring JM, Yoneda T, Weil RJ, Stark AM, Kurek R, Vega-Valle E, Feigenbaum L, and Halverson D, et al (2007). Her-2 overexpression increases the metastatic outgrowth of breast cancer cells in the brain. *Cancer Res* **67**, 4190–4198.

[22] Jensen MD, Hrinivich WT, Jung JA, Holdsworth DW, Drangova M, Chen J, and Wong E (2013). Implementation and commissioning of an integrated micro-CT RT system with computerized independent jaw collimation. *Med Phys* **40**, 081706.

[23] Thind K, Jensen MD, Hegarty E, Chen AP, Lim H, Martinez-Santiesteban F, Van Dyk J, Wong E, Scholl TJ, and Santyr GE (2014). Mapping metabolic changes associated with early radiation induced lung injury post conformal radiotherapy using hyperpolarized 13C-pyruvate magnetic resonance spectroscopic imaging. *Radiother Oncol* **110**, 317–322.

[24] Ford EC, Achanta P, Purger D, Armour M, Reyes J, Fong J, Kleinberg L, Redmond K, Wong J, and Jang MH, et al (2011). Localized CT-guided irradiation inhibits neurogenesis in specific regions of the adult mouse brain. *Radiat Res* **175**, 774–783.

[25] Wong J, Armour E, Kazanzides P, Iordachita I, Tryggestad E, Deng H, Matinfar M, Kennedy C, Liu Z, and Chan T, et al (2008). High-resolution, small animal radiation research platform with x-ray tomographic guidance capabilities. *Int J Radiat Oncol Biol Phys* **71**, 1591–1599.

[26] Clarkson R, Lindsay PE, Ansell S, Wilson G, Jelveh S, Hill RP, and Jaffray DA (2011). Characterization of image quality and image-guidance performance of a preclinical microirradiator. *Med Phys* **38**, 845.

[27] Smart D, Garcia-Glaessner A, Palmieri D, Wong-Goodrich SJ, Kramp T, Gril B, Shukla S, Lyle T, Hua E, and Cameron HA, et al (2015). Analysis of radiation therapy in a model of triple-negative breast cancer brain metastasis. *Clin Exp Metastasis* **32**, 717–727.

[28] Taskar KS, Rudraraju V, Mittapalli RK, Samala R, Thorsheim HR, Lockman J, Gril B, Hua E, Palmieri D, and Polli JW, et al (2012). Lapatinib distribution in HER2 overexpressing experimental brain metastases of breast cancer. *Pharm Res* **29**, 770–781.

[29] Morikawa A, Peereboom DM, Thorsheim HR, Samala R, Balyan R, Murphy CG, Lockman PR, Simmons A, Weil RJ, and Tabar V, et al (2014). Capecitabine and lapatinib uptake in surgically resected brain metastases from metastatic breast cancer patients: a prospective study. *Neuro Oncol* (February), 1–7.

[30] Yuan H, Gaber MW, Boyd K, Wilson CM, Kiani MF, and Merchant TE (2006). Effects of fractionated radiation on the brain vasculature in a murine model: blood-brain barrier permeability, astrocyte proliferation, and ultrastructural changes. *Int J Radiat Oncol Biol Phys* **66**, 860–866.

[31] Bart J, Groen H, Hendrikse N, van der Graaf W, Vaalburg W, and de Vries E (2000). The blood-brain barrier and oncology: new insights into function and modulation. *Cancer Treat Rev* **26**, 449–462.

[32] Madajewicz S, Chowhan N, Tfayli A, Roque C, Meek A, Davis R, Wolf W, Cabahug C, Roche P, and Manzione J, et al (2000). Therapy for patients with high grade astrocytoma using intraarterial chemotherapy and radiation therapy. *Cancer* **88**, 2350–2356.

[33] Stupp R, Hegi ME, Mason WP, van den Bent MJ, Taphoorn MJ, Janzer RC, Ludwin SK, Allgeier A, Fisher B, and Belanger K, et al (2009). Effects of radiotherapy with concomitant and adjuvant temozolomide versus radiotherapy alone on survival in glioblastoma in a randomised phase III study: 5-year analysis of the EORTC-NCIC trial. *Lancet Oncol* **10**, 459–466.